



ALMA MATER STUDIORUM  
UNIVERSITÀ DI BOLOGNA

## ARCHIVIO ISTITUZIONALE DELLA RICERCA

### Alma Mater Studiorum Università di Bologna Archivio istituzionale della ricerca

A synergic nanoantioxidant based on covalently modified halloysite-trox nanotubes with intra-lumen loaded quercetin

This is the final peer-reviewed author's accepted manuscript (postprint) of the following publication:

*Published Version:*

A synergic nanoantioxidant based on covalently modified halloysite-trox nanotubes with intra-lumen loaded quercetin / Massaro, Marina; Riela, Serena; Guernelli, Susanna; Parisi, Filippo; Lazzara, Giuseppe; Baschieri, Andrea; Valgimigli, Luca; Amorati, Riccardo. - In: JOURNAL OF MATERIALS CHEMISTRY. B. - ISSN 2050-750X. - STAMPA. - 4:(2016), pp. 2229-2241. [10.1039/c6tb00126b]

*Availability:*

This version is available at: <https://hdl.handle.net/11585/541506> since: 2020-02-25

*Published:*

DOI: <http://doi.org/10.1039/c6tb00126b>

*Terms of use:*

Some rights reserved. The terms and conditions for the reuse of this version of the manuscript are specified in the publishing policy. For all terms of use and more information see the publisher's website.

This item was downloaded from IRIS Università di Bologna (<https://cris.unibo.it/>).  
When citing, please refer to the published version.

(Article begins on next page)

This is the final peer-reviewed accepted manuscript of:

**M. Massaro, S. Riela, S. Guernelli, F. Parisi, G. Lazzara, A. Bascheri, L. Valgimigli, R. Amorati**

**A synergic nanoantioxidant based on covalently modified halloysite-trolox nanotubes with intra-lumen loaded quercetin. JOURNAL OF MATERIALS CHEMISTRY. B, 2016, vol. 4, p. 2229-2241**

The final published version is available online at: Rights / License:

<http://dx.doi.org/10.1039/c6tb00126b>

The terms and conditions for the reuse of this version of the manuscript are specified in the publishing policy. For all terms of use and more information see the publisher's website.

*This item was downloaded from IRIS Università di Bologna (<https://cris.unibo.it/>)*

***When citing, please refer to the published version.***

# Synergic Nanoantioxidant Based on Covalently Modified Halloysite-Trolox Nanotubes with Intra-lumen Loaded Quercetin

*Marina Massaro,<sup>†</sup> Serena Riela,<sup>†\*</sup> Susanna Guernelli,<sup>§</sup> Filippo Parisi,<sup>#</sup> Giuseppe Lazzara,<sup>#</sup> Andrea  
Baschieri,<sup>§</sup> Luca Valgimigli,<sup>§</sup> Riccardo Amorati<sup>§\*</sup>*

Serena Riela, e-mail: serena.riela@unipa.it; Riccardo Amorati, e-mail: riccardo.amorati@unibo.it.

<sup>†</sup>University of Palermo, Department STEBICEF, section Chemistry, Viale delle Scienze, Ed. 17, I-90128 Palermo, Italy. <sup>§</sup>University of Bologna, Department of Chemistry “G. Ciamician”, Via S. Giacomo 11, I-40126 Bologna, Italy. <sup>#</sup>University of Palermo, Department of Physic and Chemistry, Viale delle Scienze, Parco d’Orleans II, Ed. 17, 90128 Palermo, Italy.

ABSTRACT. We describe the preparation and properties of the first example of synergic nanoantioxidant, obtained by different functionalization of external surface and inner lumen of halloysite nanotubes (HNT). Trolox, a mimic of natural  $\alpha$ -tocopherol, was selectively grafted on the HNT external surface; while quercetin, a natural polyphenolic antioxidant, was loaded into the inner lumen to afford a bi-functional nanoantioxidant, HNT-Trolox/Que, which was investigated for its reactivity with transient peroxy radicals and persistent 1,1-diphenyl-2-picrylhydrazyl (DPPH $\cdot$ ) radical in comparison with the corresponding mono-functional analogues HNT-Trolox and HNT/Que. Both HNT-Trolox and HNT/Que showed good antioxidant performance in the inhibited autoxidation of organic substrates; however HNT-Trolox/Que protection by reaction with peroxy radicals was 35% higher in acetonitrile and 65% in chlorobenzene, as compared to the expected performance based on the sum of contributions of HNT-Trolox and HNT/Que. Similar enhancement was observed also in the trapping of DPPH $\cdot$  radicals. Synergism between the distinct antioxidant functions was based on the rapid reaction of externally exposed Trolox (rate constant with peroxy radicals was  $1.1 \times 10^6 \text{ M}^{-1} \text{ s}^{-1}$  and  $9 \times 10^4 \text{ M}^{-1} \text{ s}^{-1}$  respectively in chlorobenzene and acetonitrile, at 30 °C), followed by its regeneration by quercetin released from the HNT lumen. The advantages of this novel nanoantioxidant are discussed.

## INTRODUCTION

Oxidative degradation of organic materials, such as polymers, edible oils, foods and cosmetics, is due to a radical-chain mechanism, named autoxidation or lipid peroxidation, in which alkyl radicals from the substrate are converted by atmospheric O<sub>2</sub> into peroxy radicals (ROO•) that propagate the oxidative chain.<sup>1</sup> Chain-breaking antioxidants slow down the autoxidation rate by trapping ROO• radicals, as shown by equation 1, and are mainly represented by (poly)phenols, aromatic amines and some conjugated organic acids, such as ascorbic acid.<sup>2</sup>



In the continued research for new improved antioxidants, nanomaterials represent one of the most promising frontiers. Some nanomaterials, such as melanin,<sup>3</sup> V<sub>2</sub>O<sub>5</sub> nanowires<sup>4</sup> and cerium oxide<sup>5</sup> nanoparticles, show intrinsic redox activity that is often associated with radical trapping. Besides, redox inactive nanomaterials can be transformed into antioxidants by grafting low molecular weight antioxidants on them to obtain materials with improved characteristics. For instance, a covalent link between SiO<sub>2</sub> nanoparticles and gallic acid (a food-grade antioxidant) was proposed for reducing its leaching and volatility, and this material showed radical trapping activity toward the 1,1-diphenyl-2-picrylhydrazyl (DPPH•) radical.<sup>6</sup> Some of us recently demonstrated that carbon-coated cobalt nanomagnets decorated by α-tocopherol units are able to effectively counteract the autoxidation of organic substrates, and can be efficiently controlled by an external magnet.<sup>7</sup> Nanomaterials can also serve as carriers for controlled release of antioxidants. For instance, bio-degradable NPs have been used to improve the bioavailability of natural antioxidants such as epigallocatechin gallate, curcumin and quercetin.<sup>8-10</sup>

In this context, halloysite nanotubes (HNTs), a natural aluminosilicate clay, represent a versatile nanosized scaffold because chemicals can be loaded in the inner lumen, or grafted on both surfaces.<sup>11-15</sup> HNTs are a biocompatible and low cost material, with a hollow tubular structure (ca. 1  $\mu\text{m}$  in length and 80 nm in external diameter), consisting of siloxane groups on the outer surface and aluminol at the innermost surface. Therefore, the different inner and outer compositions of these materials allow exploiting different chemistry on either surface. External grafting has recently been tested by some of us in the case of curcumin, with the aim of obtaining controlled release,<sup>14,16</sup> while antioxidants loading on inner lumen has previously been reported in the case of a diarylamine for rubber stabilization,<sup>17</sup> and in the case of natural phenolic antioxidants such as curcumin,<sup>18</sup> silibinin<sup>19</sup> and resveratrol,<sup>20</sup> to obtain controlled delivery systems.

Despite the large variety of currently known antioxidants,<sup>2</sup> several challenges still exist in specific applications such as in food technology,<sup>21</sup> pharmaceutical and cosmetics' technology, or for biomedical applications, namely: (a) the potential toxicity of several antioxidants;<sup>22</sup> (b) antioxidants' leaching or migration to unwanted compartments,<sup>23</sup> which is a major challenge in food preservation<sup>24</sup> and food packaging;<sup>6</sup> (c) their thermal stability<sup>25</sup> and sensitivity to atmospheric oxygen that causes limited performance or loss of performance with time;<sup>26</sup> (d) the browning of polyphenolic antioxidants,<sup>27</sup> which might occur either enzymatically or non-enzymatically.<sup>28</sup>

For such applications the advantage of HNT-based antioxidants over conventional systems is clear: (a) halloysite is a natural material with demonstrated low toxicity both *in vitro*<sup>29</sup> and *in vivo*<sup>30</sup> and could help reduce the toxicity of small molecule antioxidants, either carried or grafted, by decreasing their steady-state concentration in the system; (b) by carrying the antioxidants, halloysite would reduce their migration and leaching; additionally, antioxidants loaded in the inner cavity might be preserved from undesired reactions such as (c) degradation under ambient O<sub>2</sub>, or (d) other unwanted reactions like polyphenols' browning.

With the aim of further improving the usefulness and the versatility of HNT-based antioxidants, we have devised the synthesis of novel HNT nanomaterials, in which different phenolic antioxidants are, for the first time, both loaded in the inner lumen and grafted on the outer surface. Indeed, the combining of different antioxidant functions on the same nanostructured material would combine the advantages outlined in points (a)-(d) and offer distinctive additional advantages, *i.e.* (e) increase the load of antioxidants hence the duration of protection, and (f) exploit any synergisms between the different antioxidants.

Synergism among antioxidants is a well known behaviour for some small-molecule compounds,<sup>31</sup> which is usually aimed at in the design of antioxidant systems for specific applications.<sup>32,33</sup> Nonetheless this approach has never been rationally explored in nanoantioxidants.

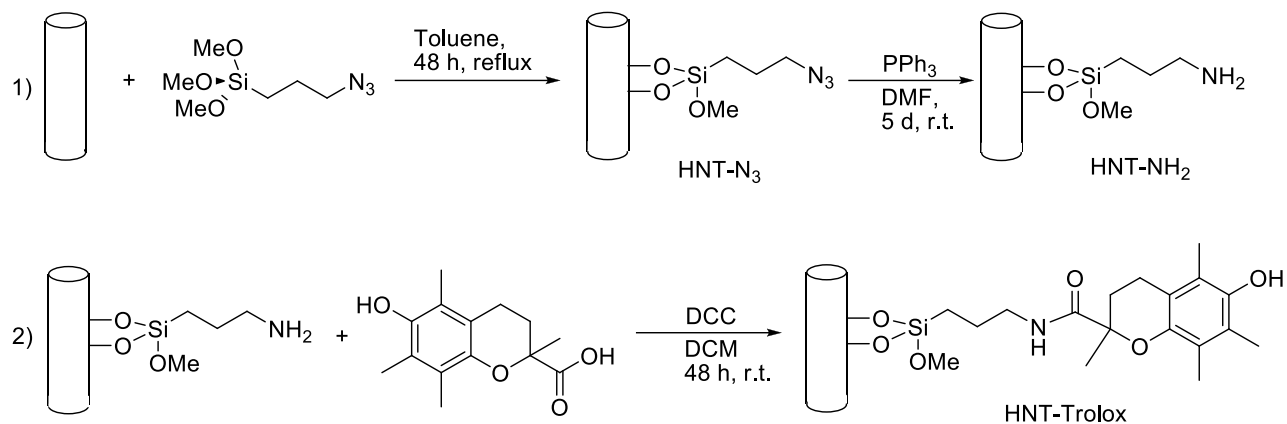
Herein we report the synthesis and characterization of a novel such HNT-based antioxidant. Trolox, a mimic of  $\alpha$ -tocopherol bearing a carboxylic group (see Scheme 1), was chosen as the surface exposed antioxidant because of its known high reactivity with radicals.<sup>6</sup> The natural polyphenol quercetin (see Scheme 2) was instead loaded in the inner lumen, because of its renown importance as radical trapping agent<sup>34</sup> and as bioactive compound to counteract oxidative stress in many pathologies.<sup>35</sup> The synergism between the two functionalities and the performance of this novel material has been investigated using both the reaction with DPPH<sup>•</sup> radicals and inhibited autoxidation studies of two model organic substrates in solvents of different polarity.

## RESULTS AND DISCUSSION

### **Synthesis of HNT-Trolox nanomaterial**

HNT bearing Trolox units was prepared according to the synthetic route shown in Scheme 1. As previously reported, halloysite nanotubes were reacted with 3-azidopropyltrimethoxysilane in toluene at reflux, affording HNT-N<sub>3</sub>, which represents a versatile starting point for subsequent

functionalizations.<sup>18</sup> The reduction with PPh<sub>3</sub> of HNT-N<sub>3</sub>, gave amino-functionalized HNT-NH<sub>2</sub><sup>14</sup> and after the work up, the NH<sub>2</sub> groups loading, estimated by TGA, was ca. 1.5±0.1 wt %.



**Scheme 1.** Schematic representation of the synthesis of HNT-Trolox nanomaterial.

The synthesis of HNT-Trolox was carried out by N,N'-dicyclohexylcarbodiimide-catalyzed condensation of Trolox to HNT-NH<sub>2</sub> by forming an amide bond that afforded a material with a loading of 8.8±0.1 wt% with respect to HNT-NH<sub>2</sub>. The new material was characterized by FT-IR spectroscopy, TGA and SEM measurements. The FT-IR spectra of HNT-Trolox, Trolox and pristine HNT are illustrated in Figure 1. The assignments for the bands of the pristine components can be done on the basis of literature data for HNT<sup>13, 36-38</sup> and Trolox.<sup>39</sup> In particular, HNTs shows two bands at 3622 and 3693 cm<sup>-1</sup> corresponding to the O–H stretching of inner hydroxyl groups and outer surface hydroxyl groups, respectively.<sup>36-38</sup> Additionally a broad signal at 1640 cm<sup>-1</sup> is attributed to the H–O–H bending of H-bonded water on the halloysite structure,<sup>36</sup> which corresponds to the broad O–H stretching signal at 3550 cm<sup>-1</sup>. Apical Si–O and Si–O–Si stretching vibrations provided the bands at 1115 and 1031 cm<sup>-1</sup>, respectively. The bands at 753 and 690 cm<sup>-1</sup> derive from the perpendicular Si–O stretching vibration. The O–H deformation vibration of inner Al–O–H groups generates the band at 912 cm<sup>-1</sup>. The FT-IR spectra of Trolox shows an intense characteristic band at ca. 3550 cm<sup>-1</sup> due to the O–H



stretching of H-bond associated phenol, while the bands at  $3015$  and  $2982\text{ cm}^{-1}$ ,  $2929$  and  $2837\text{ cm}^{-1}$  and  $2962\text{ cm}^{-1}$  are related to unsaturated CH, saturated  $\text{CH}_2$  and  $\text{CH}_3$  moieties, respectively, of the Trolox molecule. A very broad signal at  $3100\text{ cm}^{-1}$  that fuses with the C–H stretching region is due to the stretching of the H-bonded carboxylic O–H. In addition, the characteristic band at  $1720\text{ cm}^{-1}$  is ascribed to carboxylic C=O group. The hybrid material presents the characteristic bands of both HNT and Trolox with two main variations: the shift of carbonyl group from  $1720\text{ cm}^{-1}$  to  $1630\text{ cm}^{-1}$  and the disappearance of the broad signal of the C(O)O–H stretching at  $3100\text{ cm}^{-1}$ . These variations confirm the covalent grafting of Trolox to HNT-NH<sub>2</sub>, and exclude the presence of adsorbed<sup>40</sup> Trolox on the surface or in the inner lumen of the nanotubes.<sup>41</sup>

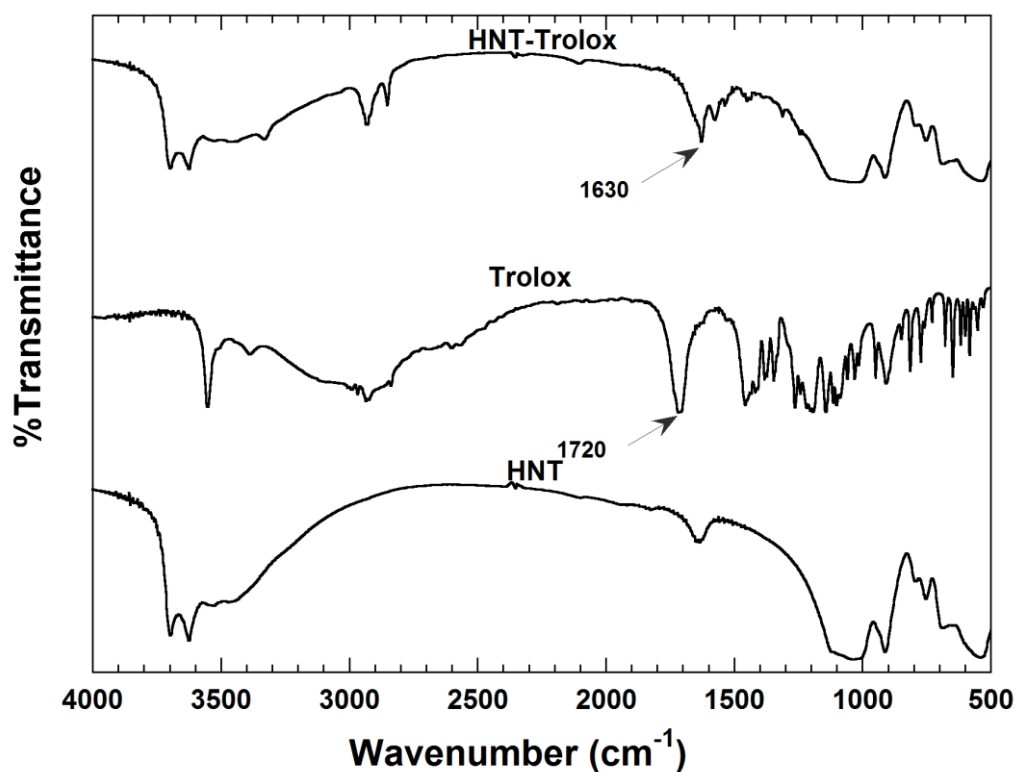


**Figure 1.** FT-IR spectra of pristine HNT, Trolox and HNT-Trolox nanomaterial.

Thermogravimetric analyses (TGA) were performed on the pristine and on the hybrid nanomaterials (thermogravimetric and derivative thermogravimetric curves are in ESI). Trolox showed a two steps degradation process, with a fast followed by a slow degradation process. The hybrid nanomaterial, had TGA profiles similar to HNT except for the thermal degradation of grafted Trolox. After the subtraction of the HNTs signal HNT-Trolox presents a mass loss vs temperature profile corresponding to that of pristine Trolox (Figure 2). This finding confirms that Trolox is attached on the external surface as its thermal stability is not significantly altered upon combination with HNT, similarly to previous observations in other surface-grafted clay materials.<sup>42,43</sup> From the mass change values it is possible to estimate the amount of Trolox grafted on HNT surface as  $10.3 \pm 0.1$  wt%. In addition to TGA analysis, to estimate the amounts of Trolox, we performed fluorescence spectroscopy experiments in methanol. The HNT-Trolox hybrid showed a characteristic fluorescence spectrum for Trolox<sup>44</sup> (see spectra in ESI) and a quantitative analysis allowed to calculate a loading of 10.4 wt%, which is in a straightforward agreement with TGA data.

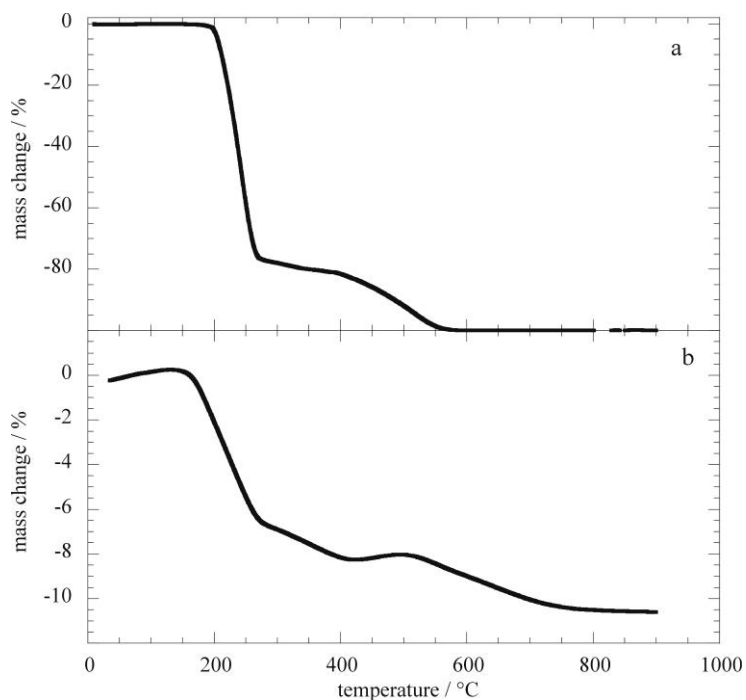


**Figure 2.** Thermogravimetric curves of Trolox (a) and HNT-Trolox after HNT signal subtraction (b).

The dimension of HNT-Trolox was assessed by dynamic light scattering (DLS) studies. The results, reported in Figure 3, show that the HNT-Trolox particles in MeCN are distributed between two populations: the first with a hydrodynamic diameter approximately around 340 nm, quite similar to the pristine HNTs, the second around a value of 1100 nm. The latter population is reasonably constituted by clusters of 3-4 HNT-Trolox units, due to the hydrophobic attractions between the Trolox molecules that are covalently linked on the surface of the HNT. Worth of note is the fact that the two populations are very well separated.

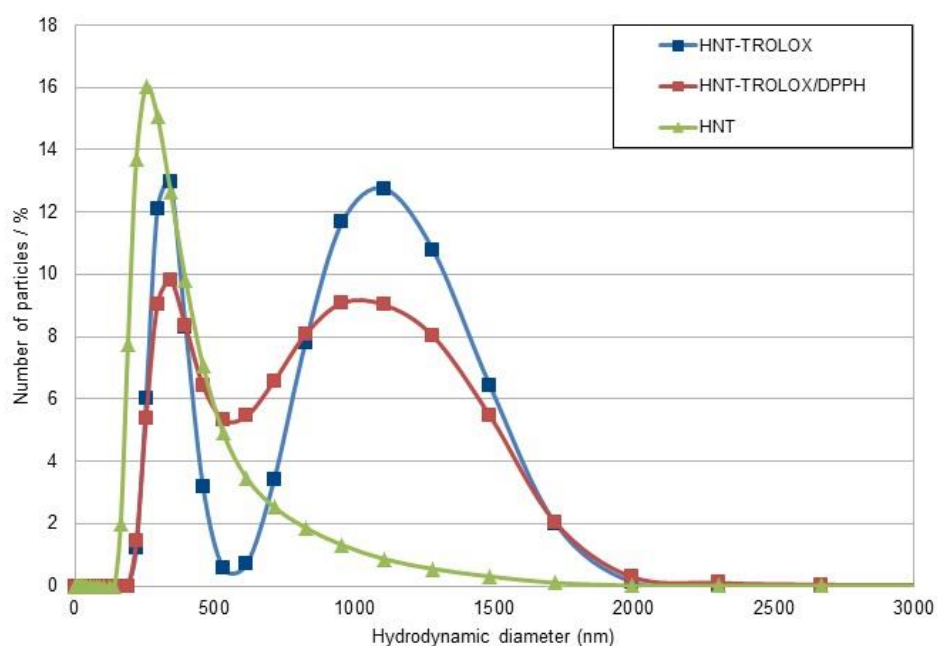


**Figure 3.** Hydrodynamic diameter distribution by DLS measurements in MeCN for pristine HNT, HNT-Trolox and HNT-Trolox treated with DPPH\* (HNT-Trolox/DPPH).

The surface morphology of HNT-Trolox was imaged by SEM. It clearly appears that the tubular shape of the halloysite is maintained after Trolox grafting (Figure 4). Furthermore the images show that

HNT-Trolox has a rather compact structure where nanotubes seem glued together as the result of interactions established by the organic structures grafted on the external surface.

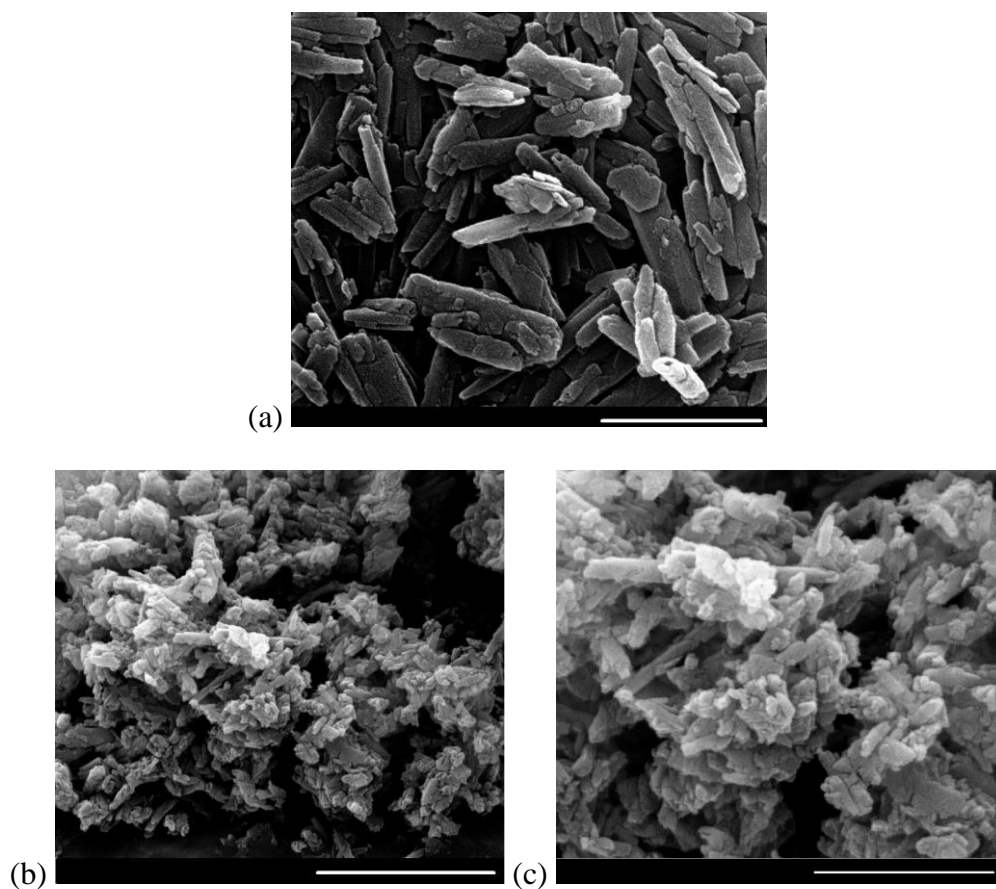


**Figure 4.** SEM images of pristine HNT (a) and of HNT-Trolox (b,c) showing the nanotubular structure ((c) enlargement of the central part of (b)), scale bars: (a) 1  $\mu\text{m}$  (b) 2  $\mu\text{m}$ ; (c) 1  $\mu\text{m}$ .

### **Loading of Quercetin into HNT-Trolox nanotubes**

With the aim of combining two or more antioxidant molecules with synergistic effects, we loaded the HNT-Trolox nanomaterial with quercetin (HNT-Trolox/Que), a polyphenolic compound that can interact with HNT lumen.<sup>19</sup>

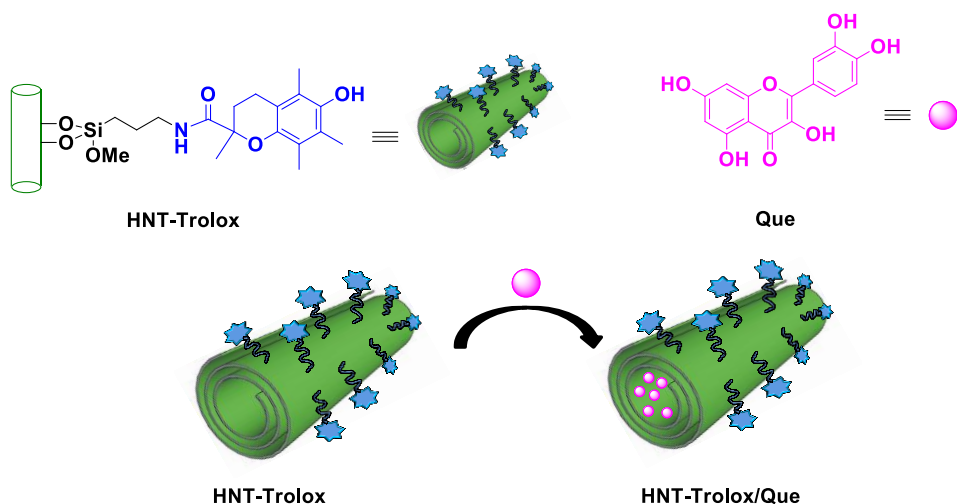


**Figure 5.** Schematic representation of quercetin loading into HNT-Trolox.

Loading quercetin into HNT-Trolox was carried out by vacuum cycling of a HNT-Trolox suspension in a quercetin solution (Figure 5). This cycle was repeated several times in order to obtain the highest loading efficiency. After loading, the HNT-Trolox/Que complex was washed with water in order to remove free quercetin. Quercetin loaded HNT without Trolox, HNT/Que, was similarly prepared as reference material. The loading efficiencies of HNT/Que and HNT-Trolox/Que were estimated spectrophotometrically after extraction with methanol. The amount of Que loaded in HNT lumen, expresses as the percent amount of drug in the final composite, was ca. 2 wt%.

The composite solid HNT-Trolox/Que was characterized by TGA. The thermoanalytical curves clearly show the successful loading of the molecule (see ESI for full details). Given that quercetin degraded with a null residual at 900 °C, we calculated that the hybrid HNT-Trolox is able to incorporate  $2.2 \pm 0.1$  wt% of quercetin by mass loss difference, in agreement with UV-vis results. It should be noted that the quercetin loading amount was unchanged for pristine HNT. It is interesting to note that quercetin was thermally stabilized by loading into either HNT or HNT-Trolox, as its thermal degradation curve was shifted toward higher temperature as compared to the native nanomaterial (Figure 6).

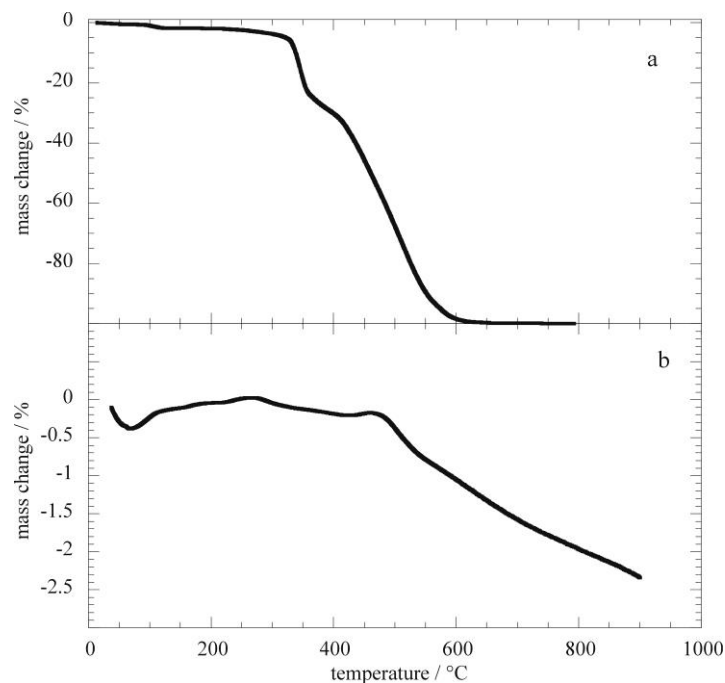


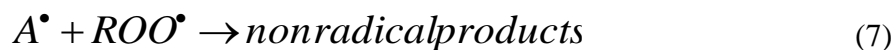
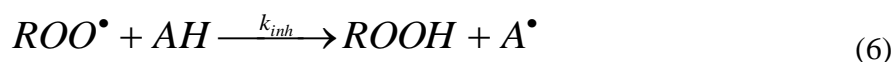
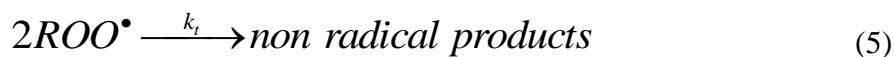
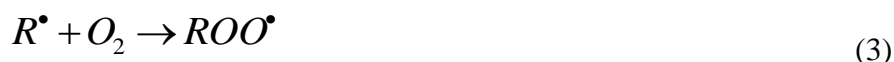
**Figure 6.** Thermogravimetric curves for quercetin (a) and nanotubes loaded with quercetin after subtraction of nanotubes signals (b).

This indicates that in the composite material quercetin is effectively loaded into the lumen. Thermal stabilization of quercetin also highlights the advantage of its loading into HNT, particularly for applications in which heating might be involved, *e.g.* during industrial processing.

### **Antioxidant activity**

Antioxidant activity of HNT-Trolox, HNT/Que and HNT-Trolox/Que was evaluated in comparison with native Trolox and quercetin, by measuring the rate constant ( $k_{inh}$ ) for the reaction with peroxy radicals ( $ROO^{\bullet}$ ), which are responsible for the propagation step of peroxidation processes in most natural and man-made materials.<sup>1</sup> The values of  $k_{inh}$  (equation 6, where AH is the antioxidant) were determined by studying the inhibition of the thermally initiated autoxidation of either cumene or styrene (RH), chosen as reference oxidizable substrates (Eqs. 2-7), under controlled conditions, using

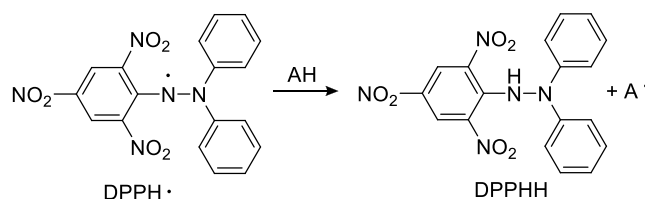
chlorobenzene or acetonitrile as solvents, which were used to simulate the apolar or mildly polar environments that can be found in the interior of biological membranes or in easily-oxidizable lipid-rich foods.<sup>45</sup>



The reactions were performed at 303 K using azobisisobutyronitrile (AIBN) as initiator, and were followed by monitoring the oxygen consumption in an oxygen-uptake apparatus based on a differential pressure transducer. In the presence of antioxidants, oxidation of the substrate and oxygen consumption are much slower than in their absence, and a clear inhibition period is observed. The rate constant for the reaction with  $ROO^\bullet$  radicals could be obtained from the rate of  $O_2$  consumption during the inhibited period from the known chain-propagation and chain-termination rate constants,  $k_p$  and  $2k_t$  respectively, for the autoxidation of styrene or cumene, as detailed in the experimental section. Styrene oxidizes quickly, similarly to the natural lipid methyl linoleate, and it is best suited to measure  $k_{inh}$  values in the range  $10^5$ - $10^7$   $M^{-1}s^{-1}$ . Cumene oxidizes slowly and can be used to measure the  $k_{inh}$  values in the range  $10^3$ - $10^5$   $M^{-1}s^{-1}$ .<sup>46</sup> The number of radicals trapped by each antioxidant molecule ( $n$ ) was obtained from the length of the inhibition period, by comparison with the reference antioxidant 2,2,5,7,8-pentamethyl-6-chromanol (PMHC), a model for the physiological antioxidant  $\alpha$ -tocopherol, for which  $n = 2$ .<sup>45</sup> In the case of HNT-Trolox and HNT-Que, the molar concentration of antioxidants (Trolox and quercetin,

respectively) could be obtained from the amount ( $w/v$ ) of nanomaterial in the sample and the loading determined by TGA.

To get a deeper insight into the radical trapping by the novel hybrid materials, we studied also the reaction with the stable coloured 1,1-diphenyl-2-picrylhydrazyl (DPPH $\cdot$ ) radical, as the purple free radical is transformed by reductants to the yellow hydrazine DPPHH through a formal hydrogen atom transfer reaction (see Scheme 2).<sup>34,47,48</sup> After mixing an excess of DPPH $\cdot$  with the investigated compounds in MeCN, the absorbance at 517 nm of DPPH $\cdot$  decreased, while the addition of pristine HNT did not modify the absorption spectrum (see ESI). The number of DPPH $\cdot$  radicals quenched by each molecule of antioxidant, free or linked to HNT, were measured from absorbance readings after 20 h of reaction, to ensure that the kinetic of release of the antioxidant from the nanoclay is not the limiting factor.



**Scheme 2.** Reaction of DPPH $\cdot$  with antioxidants.

### *Trolox and quercetin*

First, the antioxidant activities of Trolox and quercetin alone were analyzed to check the behaviour in the absence of HNT. In Figure 7A, it is evident that both Trolox and quercetin are effective inhibitors of the autoxidation of styrene in the apolar solvent PhCl, with  $k_{inh}$  values of  $9.8 \times 10^5$  and  $1.0 \times 10^6$   $M^{-1}s^{-1}$ , and stoichiometric coefficients of 1.8 and 1.9 respectively, in good agreement with previous results.<sup>46</sup>



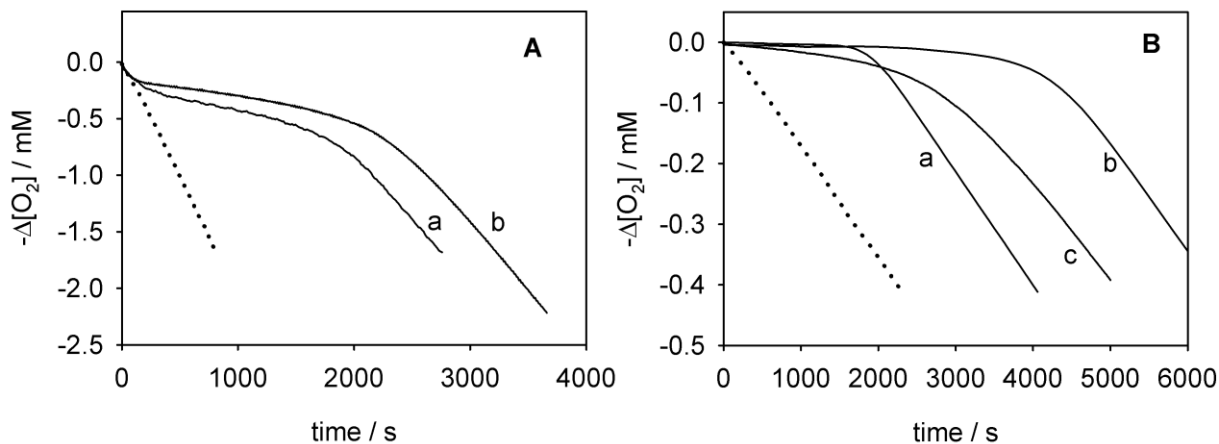
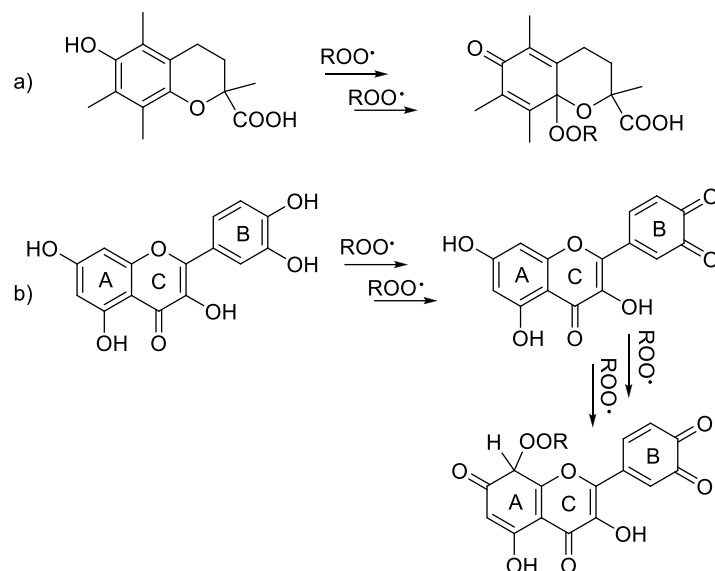


**Figure 7.** Inhibition of the autoxidation of styrene (A) or of cumene (B) in chlorobenzene by either Trolox (a) or quercetin (b), both 2.5  $\mu\text{M}$ . Trace (c) is the inhibition given by 2.5  $\mu\text{M}$  quercetin in acetonitrile. Dotted lines show the autoxidation course without antioxidants.

Parallel experiments performed by using cumene as oxidizable substrate are summarized in Figure 7B. As expected, Trolox and quercetin completely inhibited the autoxidation of cumene (traces a and b), but in the case of quercetin the stoichiometric coefficient was much larger than that recorded in the autoxidation of styrene, being about 4. This result is consistent with the capability of quercetin to efficiently trap two  $\text{ROO}^{\bullet}$  radicals by the catechol B ring, and two other radicals, more slowly, by the resorcinol A ring, as depicted in Scheme 3. The  $k_{\text{inh}}$  value relative to the second process could be distinguished in cumene, as  $5.2 \times 10^4 \text{ M}^{-1}\text{s}^{-1}$  (see Table 1).



**Scheme 3.** Stoichiometry of radical trapping by Trolox (a) and quercetin (b).

On changing the solvent from PhCl to MeCN,  $k_{\text{inh}}$  values decrease (see Table 1), due to the formation of H-bonds between MeCN and the reactive OH groups.<sup>46</sup> Comparison between traces b and c in Figure 7B shows that in MeCN the inhibiting effect of quercetin is smaller than in PhCl, and only the trapping of the first two ROO• radicals is visible.

**Table 1.** Antioxidant activity (rate constant for the reaction with ROO• radicals,  $k_{\text{inh}}$ ) and number of radicals trapped by each antioxidant molecule ( $n$ ) measured in inhibited autoxidation experiments at 303 K (mean±SD, N=3).

antioxidant	PhCl		MeCN	
	$k_{\text{inh}} / \text{M}^{-1}\text{s}^{-1}$	$n$	$k_{\text{inh}} / \text{M}^{-1}\text{s}^{-1}$	$n$
Trolox	$(9.8 \pm 0.5) \times 10^5$	$1.8 \pm 0.1$	$(1.6 \pm 0.2) \times 10^5$	$1.6 \pm 0.2$
Quercetin	$(1.0 \pm 0.1) \times 10^6$ <sup>a</sup>	$1.9 \pm 0.1$	$(1.5 \pm 0.2) \times 10^4$ <sup>a</sup>	$1.9 \pm 0.1$
HNT	No inhib.	0	No inhib.	0

Quercetin + HNT <sup>b</sup>	$(6.5 \pm 0.2) \times 10^5$	$1.3 \pm 0.2$	/	/
HNT-Trolox	$(1.1 \pm 0.1) \times 10^6$	$0.8 \pm 0.1$	$(9 \pm 2) \times 10^4$	$1.2 \pm 0.1$
HNT/Que	$(1.7 \pm 0.1) \times 10^4$ <sup>c</sup>	$1.3 \pm 0.1$	$(2.9 \pm 0.3) \times 10^3$ <sup>c</sup>	$1.4 \pm 0.1$
HNT-Trolox/Que	$(1.1 \pm 0.1) \times 10^6$	$1.5 \pm 0.2$	$(8 \pm 2) \times 10^4$	$1.9 \pm 0.2$

<sup>a</sup> Measured for the 1<sup>st</sup> reactive -OH; the value determined for the 2<sup>nd</sup> reactive -OH is  $k_{inh} (5.2 \pm 0.1) \times 10^4 \text{ M}^{-1}\text{s}^{-1}$  ( $n = 1.6 \pm 0.1$ ) and  $k_{inh} = (4.8 \pm 0.4) \times 10^3 \text{ M}^{-1}\text{s}^{-1}$  ( $n = 1.9 \pm 0.1$ ) in PhCl and MeCN respectively. <sup>b</sup> The reaction mixture contained pristine HNT (0.1 mg/mL) and variable amount of “free” quercetin. <sup>c</sup> Apparent inhibition constant; actual  $k_{inh}$  values from numerical fittings were  $1.0 \times 10^6$  and  $1.5 \times 10^4 \text{ M}^{-1}\text{s}^{-1}$  in PhCl and MeCN, respectively.

Results obtained with the DPPH<sup>•</sup> radical confirmed the stoichiometric coefficients found in the autoxidation experiments. As shown in Table 2, the stoichiometry of DPPH<sup>•</sup> radical trapping by Trolox in acetonitrile was 2, and that of quercetin was about 4.

**Table 2.** Number  $n$  of moles of DPPH<sup>•</sup> reduced per mole of antioxidant (free or linked), in acetonitrile at 298 K (mean $\pm$ SD, N=3).

Antioxidant	$n$
Trolox	$2.0 \pm 0.2$
Quercetin	$4.0 \pm 0.2$
HNT-Trolox	$1.3 \pm 0.2$
HNT/Que	$3.8 \pm 0.2$
HNT-Trolox/Que <sup>a</sup>	Expected: 1.8
	Found: $2.8 \pm 0.2$

<sup>a</sup> molar ratio trolox/quercetin = 0.79/0.21.

### HNT-Trolox nanotubes

Any of the novel HNT-based antioxidants showed good protection of styrene and cumene autoxidation, as reported in Figure 8. While pristine HNT had no effect on the autoxidation (see traces (a)), HNT-Trolox gave a strong inhibition corresponding to  $k_{inh}$  of  $1.1 \times 10^6 \text{ M}^{-1}\text{s}^{-1}$  in PhCl and  $9 \times 10^4 \text{ M}^{-1}\text{s}^{-1}$  in MeCN. These two values are very similar to those displayed by Trolox itself and indicate that the grafting on the HNT surface does not significantly modify the reactivity of the phenolic OH with  $\text{ROO}^\bullet$  radicals. On the other hand, the stoichiometry of radical trapping of HNT-Trolox, calculated on the basis of the amount of Trolox units loaded on HNT, was approximately half of that recorded for Trolox alone (see Table 1).

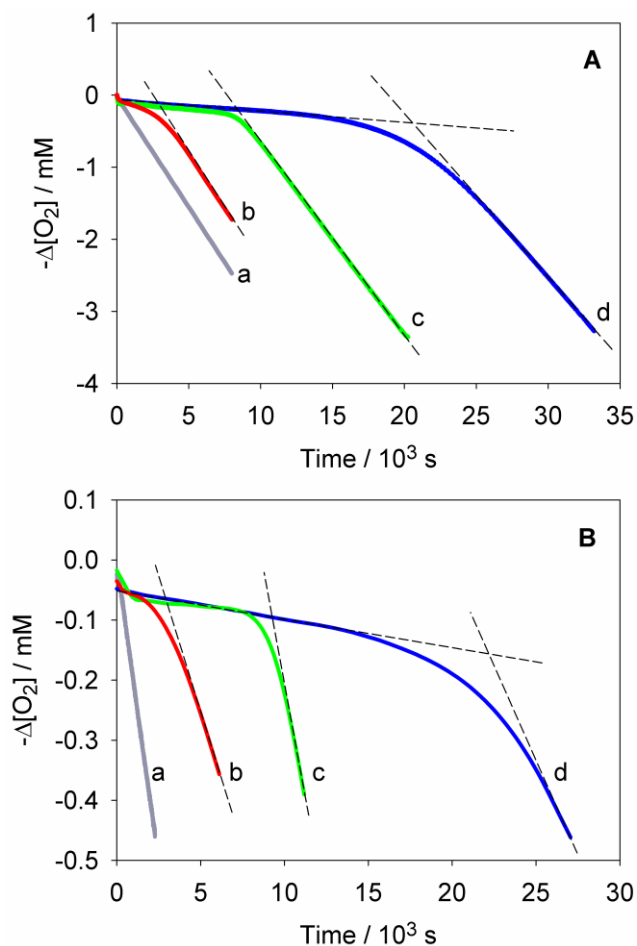


**Figure 8.** Inhibition of the autoxidation of cumene in acetonitrile (A) or chlorobenzene (B) by 0.1 mg/mL of: pristine HNT (a), HNT/Que (b), HNT-Trolox (c) and HNT-Trolox/Que (d).

Also, DPPH<sup>•</sup> experiments confirmed that the stoichiometry of HNT-Trolox is roughly half than that of Trolox (see Table 2), thus suggesting that this behaviour does not depend on the radical employed. Similar reductions of the stoichiometry after grafting an antioxidant on a nanoparticle was previously evidenced in the case of gallic acid linked to silica NPs<sup>6</sup> and Trolox linked to cobalt NPs.<sup>7</sup> As previously suggested by Deligiannakis et al., this effect is reasonably due to the preference of bound antioxidants for self-decay than for trapping a second radical.<sup>6</sup> The self-decay of phenoxyl radicals was also reported to occur between antioxidant units belonging to different nanoparticles, leading to agglomeration and to an increased hydrodynamic radius after the reaction with free radicals.<sup>6</sup> We tested this effect by performing a DLS experiment on a sample of HNT-Trolox after its reaction with an excess of DPPH<sup>•</sup>. The result, reported in Figure 3, shows that the peaks at 340 and 1100 nm of HNT-Trolox are less separated, because of the formation of some aggregates with an intermediate size. It can therefore be concluded that the reaction with DPPH<sup>•</sup> induces a slight aggregation of HNT-Trolox, reasonably due to the cross-linking of the Trolox units.

### 3) HNT/Que nanotubes

In the case of HNT-Que, the apparent antioxidant activity obtained from the slopes of the oxygen uptake plots was rather low ( $k_{inh}$  of  $1.7 \times 10^4 \text{ M}^{-1}\text{s}^{-1}$  in PhCl and  $2.9 \times 10^3 \text{ M}^{-1}\text{s}^{-1}$  in MeCN), as compared to that of quercetin itself, both in PhCl and in MeCN (Figure 8 traces (b) and Table 1). We explain this result on the basis of the low solubility and consequently slow release of quercetin from the inner lumen of HNT, so that only a small fraction of it is available for the reaction with ROO<sup>•</sup> radicals at any given time during the course of the autoxidation. To test this hypothesis, we performed autoxidation

studies inhibited by “free” quercetin in the presence of pristine HNT, and we found that in PhCl the nanoclay actively removes the antioxidant from the solution, reducing its apparent  $k_{inh}$  and  $n$  values (see Table 1). On the other hand, experiments with DPPH<sup>•</sup> showed that the stoichiometry of radical trapping of HNT-Que was very similar to that of quercetin alone in acetonitrile, reasonably because the long reaction time used in these experiments (20 h) and the excess of radical used, allowed quercetin to be almost completely released from HNT (*vide infra*).

In order to deconvolute the kinetics of release of quercetin from the kinetics of peroxy radical trapping during inhibited autoxidations, the oxygen uptake plots were analysed by numerical fitting<sup>49</sup> using a kinetic simulation software.<sup>50</sup> This analysis identified three sites for quercetin binding to HNT, L<sub>1</sub>, L<sub>2</sub> and L<sub>3</sub>, with decreasing ease of desorption by the solvent, accounting approximately for 10%, 29% and 61%, of the loaded quercetin. In the experiments in chlorobenzene, quercetin bound to L<sub>1</sub> (see Figure 9) is rapidly released during the time-course of autoxidation, whereas the quercetin bound to L<sub>2</sub> is only partially released. In acetonitrile, quercetin bound to sites L<sub>1</sub> and L<sub>2</sub> site is rapidly and almost completely released, while that bound to the high affinity site L<sub>3</sub> is negligibly released. Halloysite has specific surface area of 65 m<sup>2</sup>/g;<sup>11</sup> taking the average length of 770 nm and external diameter of 73 nm,<sup>51</sup> considering that its cavity accounts for about 10% its volume<sup>51</sup> and quercetin has molecular surface of about 70 Å<sup>2</sup>, it can be calculated that a monolayer of quercetin adsorbed in the inner lumen would account for about 1.5 wt%, in line with previous calculations for the load of monolayer surfactants.<sup>51,52</sup> This calculated value, which would correspond to 63% of the quercetin loading into HNT, is equivalent to the value of 61% obtained from our fittings for the binding site L<sub>3</sub>. We suggest that the high affinity site corresponds to the surface of the inner lumen, which is expected to bind the mildly acidic quercetin through strong H-bonding and coulombic interactions, from which it is slowly released following a solid-liquid reversible adsorption–desorption kinetics.<sup>53</sup> The intermediate affinity L<sub>2</sub> site corresponds to the solid drug accumulated in the hollow space inside HNT, which is not easily

reached by solvents, whereas the fast release site  $L_1$  corresponds to the quercetin absorbed at the ends of HNT nanotube, as depicted in Figure 9.

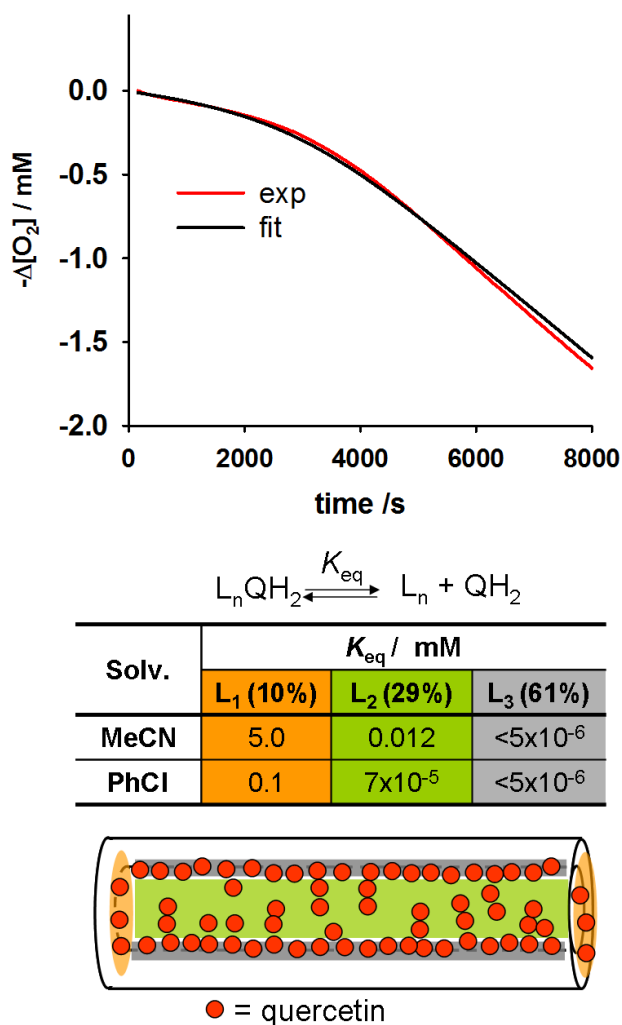


**Figure 9.** Example of the numerical analysis of  $\text{O}_2$  consumption traces. The release of quercetin ( $\text{QH}_2$ ) was simulated by assuming that it is bound to three sites, with low ( $L_1$ ), medium ( $L_2$ ) and high ( $L_3$ ) affinity.

The equilibrium constants for release of quercetin from the three binding sites are summarized in Figure 9 (see ESI for full details). HNT nanotubes serve as controlled release systems for loaded

quercetin, which displays the typical reactivity with peroxy radicals after release in solution:  $k_{inh}$  of  $1.0 \times 10^6 \text{ M}^{-1}\text{s}^{-1}$  in PhCl and  $1.5 \times 10^4 \text{ M}^{-1}\text{s}^{-1}$  in MeCN.

This explanation was supported by UV-Vis spectroscopy measurements in MeCN (see ESI), which showed a fast release of 35% quercetin in about two hours, followed by a much slower release which accounted for only an additional 2% of quercetin released after 20 hours.

Under these conditions, experimental data points can be analyzed with the following equation:

$$Abs(t) = A_1 [1 - e^{(-k_1 t)}] + k_0 t \quad (8)$$

comprising the sum of an exponential and a linear term. This indicates the superimposition of two distinct processes, namely a relatively faster first-order ( $k_1 = 0.077 \pm 0.007 \text{ min}^{-1}$ ) and a much slower zero-order release ( $k_0 = 0.0022 \pm 0.0009 \text{ min}^{-1}$ ).

These results suggest that HNT/Que acts as a dynamic reservoir of quercetin, whose release in solution is regulated by its consumption by the oxidizing radicals. This also explains the higher apparent stoichiometric factor recorded for reaction with persistent DPPH<sup>•</sup> radical (see Table 2), which “waits” in solution until all quercetin has been released, by shifting its equilibrium of binding with the nanotube.

#### 4) HNT-Trolox/Que hybrid nanotubes

HNT-Trolox/Que showed a very strong antioxidant activity both in PhCl and in MeCN, as can be inferred from traces (d) in Figure 8. Interestingly, both the inhibition length and efficacy was higher than the sum of effects observed for HNT-Trolox and HNT/Que, indicating the occurrence of synergy between the two antioxidant functions in HNT-Trolox/Que. In fact, the number of theoretical radicals trapped by a solution of HNT-Trolox/Que (with a molar ratio 0.79/0.21 for Trolox/Quercetin) without synergic effect would be  $n_{Theor} = 1.24$  in MeCN, using  $n = 1.2$  for HNT-Trolox and  $n = 1.4$  for HNT/Que; instead the radicals trapped by our new of three-component system are  $n_{Exp} = 1.9$  in MeCN,



which is greater than  $n_{\text{Theor}}$ , as visually shown in Figure 10. Similarly, in PhCl  $n_{\text{Exp}} = 1.5$  is higher than the theoretical value  $n_{\text{Theor}} = 0.91$ .

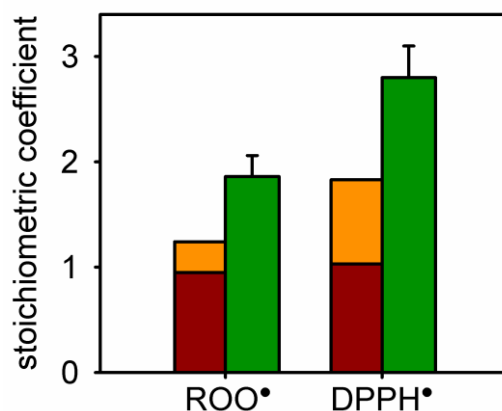
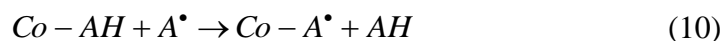
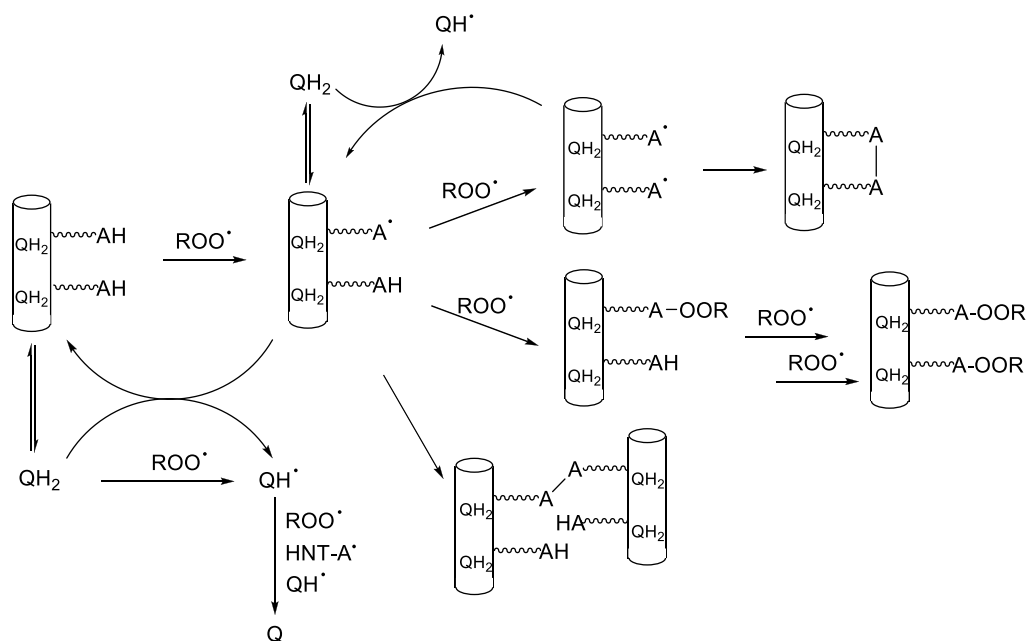


**Figure 10.** Synergic effect in HNT-Trolox/Que: experimental stoichiometric coefficient in MeCN (green bars,  $\pm$ SD, N=3) compared to theoretic one, as calculated from the sum of contributions of HNT-Trolox (red bars) and HNT/Que (orange bars) alone.

The synergic effect is also observed in DPPH• experiments: radicals trapped by HNT-Trolox/Que are  $n_{\text{Exp}} = 2.8$  in MeCN, a value much greater than  $n_{\text{Theor}} = 1.9$  (see Figure 10), that can be calculated using  $n = 1.3$  for HNT-Trolox and  $n = 3.8$  for HNT/Que. Interestingly, the length of the antioxidant activity of mixtures of Trolox and quercetin was the sum of the contributions of the single components (see ESI). Synergic antioxidant effect has previously been observed for antioxidant mixtures in solution and is typical of a main (*i.e.* more active) antioxidant AH being regenerated from its oxidation products by a co-antioxidant Co-AH acting as a sacrificial reducing agent<sup>33,54</sup> as simplified in eq. 9-10.



In the case of HNT-Trolox/Que antioxidant system, kinetic analysis indicates that Trolox grafted on HNT surface acts as main antioxidant (AH) being immediately available for fast reaction with peroxy radicals, then it is regenerated by quercetin, the co-antioxidant, which is slowly released from the nanotube cavity. However, as the grafting of Trolox on HNT reduces its stoichiometric coefficient, similarly to all known examples of surface-bound antioxidants, the effect of loaded quercetin appears that of restoring the pristine radical trapping ability of Trolox. Therefore, the synergic interplay between the two antioxidant functions is a distinctive advantage of this novel nano-antioxidant since it is able to afford rapid protection from oxidation using externally exposed Trolox, combined with prolonged undiminished efficacy due to the slow release of loaded quercetin, which is mainly regulated by its rate of consumption to regenerate the main antioxidant. An account of the different radical reactions involved in the antioxidants activity of HNT-Trolox/Que is reported in Scheme 4.



**Scheme 4.** Mechanism explaining the antioxidant behaviour of HNT-Trolox/Que, where Trolox is identified as AH and quercetin as QH<sub>2</sub>.

## CONCLUSIONS

HNT-Trolox/Que is a very effective antioxidant nanomaterial, endowed with complementary antioxidant functionalities displaying synergistic effects. To the best of our knowledge, this is the first example of a synergic nanoantioxidant. It also represents the prototype for a general design strategy expected to afford improved antioxidant halloysite nanotubes, in which one main phenolic antioxidant function (like Trolox) is exposed on the outer surface and is readily available to trap free radicals, whereas a second co-antioxidant (like quercetin) is loaded in the inner lumen and is slowly released to regenerate the main antioxidant and afford a prolonged synergistic protection. We have shown that both HNT-Trolox and HNT/Que are interesting and effective antioxidant materials, able to quench both DPPH<sup>•</sup> and peroxy radicals, protecting organic materials from autoxidations. However, their stoichiometry of radical trapping is less favourable than results obtained with the corresponding molecular antioxidants (*i.e.* “free” Trolox or quercetin); similar unfavourable feature has previously been reported for nano-antioxidants built by functionalization of a nanosized scaffold with a phenolic compound.<sup>6,7</sup> In this respect we showed that HNT-Trolox/Que offers a distinctive advantage in that, due to the synergistic interplay among antioxidant functions, it offers extended protection with respect of materials endowed with a single antioxidant function.

## EXPERIMENTAL SECTION

**Materials.** Trolox, quercetin, styrene, cumene, AIBN were commercially available (Sigma Aldrich). Solvents were of the highest grade commercially available and were used as received. Styrene and cumene were percolated twice on an alumina column before use. AIBN was recrystallized from methanol and stored at -18 °C. All reagents needed for the functionalization (Sigma) were used without further purification.

Halloysite was purchased from Sigma-Aldrich. This material has an average tube diameter of 50 nm and inner lumen diameter of 15 nm. Typical specific surface area of this halloysite is  $65 \text{ m}^2 \text{ g}^{-1}$ ; pore volume of  $\sim 1.25 \text{ cm}^3 \text{ g}^{-1}$ ; refractive index 1.54 and specific gravity  $2.53 \text{ g cm}^{-3}$ .

**Synthesis of HNT-Trolox.** HNT-N<sub>3</sub> and HNT-NH<sub>2</sub> were prepared as previously reported.<sup>14,18</sup> ( $\pm$ )-6-hydroxy-2,5,7,8-tetramethylchromane-2-carboxylic acid (55 mg, 10 eq) was suspended in CH<sub>2</sub>Cl<sub>2</sub> (7.5 mL) and N,N dicyclohexylcarbodiimide (88 mg, 10 eq) was added. The suspension was stirred under argon atmosphere, at room temperature for 10 min. Afterwards HNT-NH<sub>2</sub> (250 mg) was quickly added. The mixture was left under stirring for 48h. Then, the solvent was filtered off, the powder was rinsed with H<sub>2</sub>O and, successively, with CH<sub>2</sub>Cl<sub>2</sub> and finally dried at 80 °C under vacuum.

**Loading of quercetin.** To a dispersion of HNT or HNT-Trolox in deionized water (5 mL), 1 mL of quercetin solution  $10^{-2} \text{ M}$  in ethanol was added. The suspension was sonicated for 5 min, at an ultrasound power of 200 W and at 25 °C and then was evacuated for 3 cycles. The suspension was left under stirring for 24 h at room temperature. After this time the powder was washed with water and then dried at 70 °C under vacuum. Loading was determined as follows: ca. 5 mg of HNT or HNT-Trolox were carefully weighed and washed with methanol (25 mL). The quercetin concentration in solution was determined by UV-vis spectrometry using the Lambert-Beer law.

**General procedures.** Dynamic light scattering (DLS) measurements were carried out by means of a Zetasizer NANO-ZS (Malvern Instruments). The field-time autocorrelation functions were analyzed by the Inverse Laplace Transform (ILT), which provides the decay rates ( $\Gamma$ ) of the diffusive modes. For the translational motion, the collective diffusion coefficient at a given concentration is  $D_t = \Gamma/q^2$  where  $q$  is the scattering vector given by  $4 \pi n \lambda^{-1} \sin(\theta/2)$  being  $n$  the acetonitrile refractive index,  $\lambda$  the wavelength (632.8 nm) and  $\theta$  the scattering angle (173°). The Hydrodynamic diameter ( $D_h$ ) was calculated by means of Stokes-Einstein relation. The thermogravimetric analyses were done by using a

Q5000 IR apparatus (TA Instruments) under nitrogen flow of  $25 \text{ cm}^3 \text{ min}^{-1}$  for the sample and  $10 \text{ cm}^3 \text{ min}^{-1}$  for the balance at the heating rate of  $10 \text{ }^\circ\text{C min}^{-1}$ . Temperature spanned from ambient to  $900 \text{ }^\circ\text{C}$ . FT-IR spectra in KBr were determined at room temperature in the spectral region  $400\text{--}4000 \text{ cm}^{-1}$  by means of an FT-IR spectrophotometer (Agilent Technologies Cary 630). An average of 30 scans per sample using a nominal resolution of  $4 \text{ cm}^{-1}$  was registered. An AESEM FEI QUANTA 200F microscope apparatus was used to study the morphology of the functionalized HNTs. Before each experiment, the sample was coated with gold under argon by means of an Edwards Sputter Coater S150A, in order to avoid charging under electron beam. Fluorescence experiments were carried out in a Fluoromax 4 (Jobin- Yvon) spectrofluorometer (right angle geometry,  $1 \text{ cm} \times 1 \text{ cm}$  quartz cell) at  $25.0 \text{ }^\circ\text{C}$ . The excitation wavelength was of  $290 \text{ nm}$  and the emission spectra were recorded from  $300$  to  $500 \text{ nm}$ . The widths of slits were set at  $2$  and  $2 \text{ nm}$  for excitation and emission, respectively. Long pass filter was used to suppress HNT scattered radiation. UV-vis spectra were performed with a Beckmann DU 650 spectrometer.

**Antioxidant activity.** The chain-breaking antioxidant activity of the title compounds was evaluated by studying the inhibition of the thermally initiated autoxidation of styrene ( $4.3 \text{ M}$ ) or cumene ( $3.5 \text{ M}$ ) in chlorobenzene or acetonitrile. Autoxidation experiments were performed by measuring the  $\text{O}_2$  consumption by a gas-uptake recording apparatus built in our laboratory based on a Validyne DP15 differential pressure transducer.<sup>55</sup> In a typical experiment, an air-saturated mixture of the oxidizable substrate and the solvent containing AIBN ( $0.025 \text{ M}$ ) was equilibrated with the reference solution containing also an excess of 2,2,5,7,8-pentamethyl-6-chromanol in the same solvent at  $30 \text{ }^\circ\text{C}$ . After equilibration,  $50\text{--}150 \text{ }\mu\text{L}$  of a concentrated solution of the antioxidant was injected into the sample flask, and the oxygen consumption in the sample was measured. From the slope of the oxygen consumption during the inhibited period (see Figures 7 and 8),  $k_{\text{inh}}$  values were obtained by using

equation 11 while the  $n$  coefficients were determined from the length of the inhibited period ( $\tau$ ) by using equation 12, from the known rate of radical production by AIBN (initiation rate,  $R_i$ ).

$$\Delta[O_2]_t = -\frac{k_p}{k_{inh}} \cdot [cumene] \cdot \ln\left(\frac{1-t}{\tau}\right) \quad (\text{eq. 11})$$

$$n = \frac{R_i \cdot \tau}{[\text{antioxidant}]} \quad (\text{eq. 12})$$

The  $k_p$  values of styrene and cumene at 303 K are 41 and  $0.32 \text{ M}^{-1}\text{s}^{-1}$ , respectively. The value of  $R_i$  was determined in each experimental condition by using 2,2,5,7,8-pentamethyl-6-chromanol ( $n=2$ ) as a reference.<sup>45,46</sup>

**Determination of DPPH<sup>•</sup> scavenging.** The reaction mixtures were prepared by adding to DPPH<sup>•</sup> radical in acetonitrile ( $1.0 \times 10^{-4}$  and  $5.0 \times 10^{-5}$  M) different concentrations of the investigated radical. Total volume of the reaction mixture was 2 mL. Absorption of DPPH<sup>•</sup> was determined by recording spectra in sequence until the absorbance was unchanged (20 h) and against a blank solution that contained only acetonitrile ( $\lambda_{\text{max}} = 517 \text{ nm}$ ,  $\epsilon = 11000 \pm 50$ ).<sup>34</sup> UV-vis spectra were recorded by a Jasco V-550 spectrophotometer.

## ASSOCIATED CONTENT

**Electronic Supplementary Information (ESI).** FT-IR and TGA of novel materials, examples of UV traces for experiments with DPPH<sup>•</sup>, release profile of quercetin from HNT/Que, examples of numerical fittings of oxygen uptake kinetics.

## ACKNOWLEDGMENT

This work was supported by a grant to L.V., A.B., and R.A. from the Italian MIUR (PRIN 2010-2011 2010PFLRJR, PROxi project). L.V. and R.A. acknowledge funding from the University of Bologna (FARB project FFBO123154) and support from COST action CM1201. We acknowledge also support

from the University of Palermo, PRIN 2010-2011 (prot. 2010329WPF), FIRB 2012 (prot. RBFR12ETL5), PON-TECLA (PON03PE\_00214\_1).

## ABBREVIATIONS

HNT, halloysite nanotubes; ROO<sup>•</sup>, alkylperoxyl radical; DPPH<sup>•</sup>, diphenylpicrylhydrazyl radical; DLS, dynamic light scattering; TGA, thermo-gravimetric analysis; AIBN, 2,2'-azobis(isobutyronitrile).

## REFERENCES

- 1) R. Amorati and L. Valgimigli, Advantages and limitations of common testing methods for antioxidants, *Free Radic. Res.* **2015**, *49*, 633–649.
- 2) K. U. Ingold and D. A. Pratt, Advances in radical-trapping antioxidant chemistry in the 21st century: a kinetics and mechanisms perspective, *Chem. Rev.* **2014**, *114*, 9022–9046.
- 3) E. Kim, Y. Liu, W. T. Leverage, J.-J. Yin, I. M. White, W. E. Bentley and G. F. Payne, Context-dependent redox properties of natural phenolic materials, *Biomacromolecules* **2014**, *15*, 1653–1662
- 4) A. A. Vernekar, D. Sinha, S. Srivastava, P. U. Paramasivam, P. D'Silva and G. Mugesh, An antioxidant nanozyme that uncovers the cytoprotective potential of vanadia nanowires. *Nat. Commun.* **2014**, *5*, 5301.
- 5) S. S. Lee, W. Song, M. Cho, H. L. Puppala, P. Nguyen, H. Zhu, L. Segatori and V. L. Colvin, Antioxidant properties of cerium oxide nanocrystals as a function of nanocrystal diameter and surface coating, *ACS nano* **2013**, *7*, 9693–9703
- 6) Y. Deligiannakis, G. A. Sotiriou and S. E. Pratsinis, Antioxidant and antiradical SiO<sub>2</sub> nanoparticles covalently functionalized with gallic acid, *ACS Appl. Mater. Interfaces* **2012**, *4*, 6609–6617.

- 7) C. Viglianisi, V. Di Pilla, S. Menichetti, V. M. Rotello, G. Candiani, C. Malloggi and R. Amorati, Linking an  $\alpha$ -tocopherol derivative to cobalt(0) nanomagnets: magnetically responsive antioxidants with superior radical trapping activity and reduced cytotoxicity, *Chem. Eur. J.* **2014**, *20*, 6857–6860.
- 8) B. Hu, Y. Ting, X. Zeng and Q. Huang, Bioactive peptides/chitosan nanoparticles enhance cellular antioxidant activity of (–)-epigallocatechin-3-gallate, *J. Agric. Food Chem.* **2013**, *61*, 875–881.
- 9) X. Xie, Q. Tao, Y. Zou, F. Zhang, M. Guo, Y. Wang, H. Wang, Q. Zhou and S. Yu, PLGA nanoparticles improve the oral bioavailability of curcumin in rats: characterizations and mechanisms, *J. Agric. Food Chem.* **2011**, *59*, 9280–9289.
- 10) A. Kumari, S. K. Yadav, Y. B. Pakade, B. Singh and S. C. Yadav, Development of biodegradable nanoparticles for delivery of quercetin, *Colloid Surfaces B*, **2010**, *80*, 184–192.
- 11) Y. M. Lvov, D. G. Shchukin, H. Mohwald and R. R. Price, Halloysite clay nanotubes for controlled release of protective agents, *ACS nano* **2008**, *2*, 814–820.
- 12) H. Zhang, T. Ren, Y. Ji, L. Han, Y. Wu, H. Song, L. Bai and X. Ba, Selective modification of halloysite nanotubes with 1-pyrenylboronic acid: a novel fluorescence probe with highly selective and sensitive response to hyperoxide, *ACS Appl. Mater. Interf.* **2015**, *7*, 23805–23811.
- 13) F. Arcudi, G. Cavallaro, G. Lazzara, M. Massaro, S. Milioto, R. Noto and S. Riela, Selective functionalization of halloysite cavity by click reaction: structured filler for enhancing mechanical properties of bionanocomposite films, *J. Phys. Chem. C* **2014**, *118*, 15095–15101.
- 14) G. Cavallaro, G. Lazzara, M. Massaro, S. Milioto, R. Noto, F. Parisi and S. Riela, Biocompatible poly(N-isopropylacrylamide)-halloysite nanotubes for thermoresponsive curcumin release, *J. Phys. Chem. C* **2015**, *119*, 8944–8951.
- 15) N. G. Veerabadran, D. Mongayt, V. Torchilin, R. R. Price and Y. M. Lvov, Organized shells on clay nanotubes for controlled release of macromolecules. *Macromol. Rapid Commun.* **2009**, *30*, 99–103



- 16) M. Massaro, R. Amorati, G. Cavallaro, S. Guernelli, G. Lazzara, S. Milioto, R. Noto, P. Poma and S. Riela. Direct chemical grafted curcumin on halloysite nanotubes as dual-responsive prodrug for pharmacological applications. *Colloid Surface B*, **2016**, *140*, 505–513
- 17) Y. Fu, D. Zhao, P. Yao, W. Wang, L. Zhang and Y. Lvov, Highly aging-resistant elastomers doped with antioxidant-loaded clay nanotubes, *ACS Appl. Mater. Interfaces* **2015**, *7*, 8156–8165.
- 18) S. Riela, M. Massaro, C. G. Colletti, A. Bommarito, C. Giordano, S. Milioto, R. Noto, P. Poma and G. Lazzara, Development and characterization of co-loaded curcumin/triazole-halloysite systems and evaluation of their potential anticancer activity, *Int. J. Pharm.* **2014**, *475*, 613–623.
- 19) M. Massaro, S. Piana, C. G. Colletti, R. Noto, S. Riela, C. Baiamonte, C. Giordano, G. Pizzolanti, G. Cavallaro, S. Milioto and G. Lazzara, Multicavity halloysite–amphiphilic cyclodextrin hybrids for co-delivery of natural drugs into thyroid cancer cells, *J. Mater. Chem. B* **2015**, *3*, 4074-4081.
- 20) V. Vergaro, Y. M. Lvov and S. Leporatti, Halloysite clay nanotubes for resveratrol delivery to cancer cells, *Macromol. Biosci.* **2012**, *12*, 1265–1271.
- 21) A. L. Chun, Will the public swallow nanofood? *Nat. Nanotechnol.* **2009**, *4*, 790-791.
- 22) R. Amorati, M. C. Foti and L. Valgimigli, Antioxidant activity of essential oils, *J. Agric. Food Chem.* **2013**, *61*, 10835–10847.
- 23) J. A. Garde, R. Catalá, R. Gavara and R. J. Hernandez, Characterizing the migration of antioxidants from polypropylene into fatty food simulants, *Food Addit. Contam.* **2001**, *18*, 750-762.
- 24) E. A. Decker, K. Warner, M. P. Richards and F. Shahidi, Measuring antioxidant effectiveness in food, *J. Agric. Food. Chem.* **2005**, *53*, 4303-4310.
- 25) J. M. Cruz, E. Conde, H. Domínguez and J. C. Parajó, Thermal stability of antioxidants obtained from wood and industrial wastes, *Food Chem.* **2007**, *100*, 1059–1064.
- 26) L. Valgimigli and D. A. Pratt, Maximizing the reactivity of phenolic and aminic radical-trapping antioxidants: just add nitrogen!, *Acc. Chem. Res.* **2015**, *48*, 966–975.

- 27) C. Queiroz, A. J. Ribeiro da Silva, M. L. Mendes Lopes, E. Fialho and V. L. Valente-Mesquita, Polyphenol oxidase activity, phenolic acid composition and browning in cashew apple (*Anacardium occidentale*, L.) after processing, *Food Chem.* **2011**, *125*, 128–132.
- 28) L. Manzocco, S. Calligaris, D. Mastrocola, M. C. Nicoli and C. R. Lerici, Review of nonenzymatic browning and antioxidant capacity in processed foods, *Trends Food Sci. Technol.* **2001**, *11*, 340–346.
- 29) V. Vergaro, E. Abdullayev, Y. M. Lvov, A. Zeitoun, R. Cingolani, R. Rinaldi and S. Leporatti Cytocompatibility and uptake of halloysite clay nanotubes, *Biomacromolecules* **2010**, *11*, 820–826.
- 30) G. I. Fakhrullina, F. S. Akhatova, Y. M. Lvov and R. F. Fakhrullin, Toxicity of halloysite clay nanotubes *in vivo*: a *caenorhabditis elegans* study, *Environ. Sci.: Nano*, **2015**, *2*, 54-59.
- 31) L. Valgimigli, M. Lucarini, G. F. Pedulli and K. U. Ingold, Does  $\beta$ -carotene really protect vitamin E from oxidation?, *J. Am. Chem. Soc.* **1997**, *119*, 8095-8096.
- 32) S. Kumar, H. Johansson, L. Engman, L. Valgimigli, R. Amorati, M. G. Fumo and G. F. Pedulli, Regenerable chain-breaking 2,3-dihydrobenzo[b]selenophene-5-ol antioxidants, *J. Org. Chem.* **2007**, *72*, 2583-2595.
- 33) L. Valgimigli, D. Bartolomei, R. Amorati, E. Haidasz, J. J. Hanthorn, S. J. Nara, J. Brinkhorst and D. A. Pratt, 3-Pyridinols and 5-pyrimidinols: tailor-made for use in synergistic radical-trapping co-antioxidant systems, *Beilstein J. Org. Chem.* **2013**, *9*, 2781–2792.
- 34) M. C. Foti, C. Daquino, G. A. Di Labio and K. U. Ingold Kinetics of the oxidation of quercetin by 1,1-diphenyl-2-picrylhydrazyl (dpph•), *Org. Lett.* **2011**, *13*, 4826-4829.
- 35) M. Russo, C. Spagnuolo, I. Tedesco, S. Bilotto and G. L. Russo, The flavonoid quercetin in disease prevention and therapy: facts and fancies, *Biochem. Pharmacol.* **2012**, *83*, 6–15.
- 36) P. Djongoue and D. Njopwouo, FT-IR spectroscopy applied for surface clays characterization, *Journal of Surface Engineered Materials and Advanced Technology*, **2013**, *3*, 275-282.

- 37) K. P. Nicolini, C. R. B. Fukamachi, F. Wypych and A. S. Mangrich; Dehydrated halloysite intercalated mechanochemically with urea: thermal behavior and structural aspects, *J. Colloid Interf. Sci.* **2009**, *338*, 474–479.
- 38) É. Makó, J. Kristóf, E. Horváth and V. Vágvölgyi, Kaolinite–urea complexes obtained by mechanochemical and aqueous suspension techniques - a comparative study, *J. Colloid Interf. Sci.* **2009**, *330*, 367–373.
- 39) L. Gastaldi, E. Ugazio, S. Sapino, P. Iliade, I. Miletto and G. Berlier, Mesoporous silica as a carrier for topical application: the Trolox case study, *Phys. Chem. Chem. Phys.* **2012**, *14*, 11318–11326.
- 40) M. Massaro, C. G. Colletti, R. Noto, S. Riela, P. Poma, S. Guernelli, F. Parisi, S. Milioto and G. Lazzara, Pharmaceutical properties of supramolecular assembly of co-loaded cardanol/triazole-halloysite systems, *Int. J. Pharm.* **2015**, *478*, 476–485.
- 41) G. Cavallaro, G. Lazzara and S. Milioto, Exploiting the colloidal stability and solubilization ability of clay nanotubes/ionic surfactant hybrid nanomaterials, *J. Phys. Chem. C* **2012**, *116*, 21932–21938.
- 42) P. Yuan, P. D. Southon, Z. Liu, M. E. R. Green, J. M. Hook, S. J. Antill and C. J. Keper, Functionalization of halloysite clay nanotubes by grafting with  $\gamma$ -aminopropyltriethoxysilane, *J. Phys. Chem. C* **2008**, *112*, 15742–15751.
- 43) W. Shen, H. He, J. Zhu, P. Yuan and R. L. Frost, Grafting of montmorillonite with different functional silanes via two different reaction systems, *J. Colloid Interface Sci.* **2007**, *313*, 268–273.
- 44) S. A. V. Eremia, D. Chevalier-Lucia, G.-L. Radu, J.-L. Marty, Optimization of hydroxyl radical formation using TiO<sub>2</sub> as photocatalyst by response surface methodology, *Talanta*, **2008**, *77*, 858–862.
- 45) R. Amorati, G. F. Pedulli and L. Valgimigli, Kinetic and thermodynamic aspects of the chain-breaking antioxidant activity of ascorbic acid derivatives in non-aqueous media, *Org. Biomol. Chem.* **2011**, *9*, 3792–3800.

- 46) R. Amorati, L. Valgimigli, L. Panzella, A. Napolitano and M. d'Ischia, 5-S-Lipoylhydroxytyrosol, a multidefense antioxidant featuring a solvent-tunable peroxy radical-scavenging 3-thio-1,2-dihydroxybenzene motif, *J. Org. Chem.* **2013**, *78*, 9857–9864.
- 47) M. Musialik and G. Litwinienko, Scavenging of dpph<sup>\*</sup> radicals by vitamin E is accelerated by its partial ionization: the role of sequential proton loss electron transfer, *Org. Lett.* **2005**, *7*, 4951-4954.
- 48) M. Musialik, R. Kuzmicz, T. S. Pawłowski and G. Litwinienko, Acidity of hydroxyl groups: an overlooked influence on antiradical properties of flavonoids, *J. Org. Chem.* **2009**, *74*, 2699–2709.
- 49) R. Amorati, P. T. Lynett, L. Valgimigli and D. A. Pratt, The reaction of sulfenic acids with peroxy radicals: insights into the radical-trapping antioxidant activity of plant-derived thiosulfonates, *Chem. Eur. J.* **2012**, *18*, 6370 – 6379.
- 50) P. Mendes, Biochemistry by numbers: simulation of biochemical pathways with Gepasi 3, *Trends Biochem. Sci.* **1997**, *22*, 361-363.
- 51) G. Cavallaro, G. Lazzara, S. Milioto, G. Palmisano and F. Parisi, Halloysite nanotube with fluorinated lumen: non-foaming nanocontainer for storage and controlled release of oxygen in aqueous media, *J. Colloid Interf. Sci.* **2014**, *417*, 66–71.
- 52) L. Nordstierna, I. Furo' and P. Stilbs, Mixed adsorption of fluorinated and hydrogenated surfactants, *Langmuir* **2006**, *22*, 7969-7974.
- 53) C. Aguzzi, C. Viserasa, P. Cerezo, I. Salcedo, R. Sánchez-Espejo and C. Valenzuela, Release kinetics of 5-aminosalicylic acid from halloysite, *Colloids Surf. B* **2013**, *105*, 75– 80.
- 54) S. Kumar, H. Johansson, T. Kanda, L. Engman, T. Müller, H. Bergenudd, M. Jonsson, G. F. Pedulli, R. Amorati and L. Valgimigli, Catalytic chain-breaking pyridinol antioxidants, *J. Org. Chem.* **2010**, *75*, 716–725.
- 55) M. Lucarini, G. F. Pedulli, L. Valgimigli and R. Amorati, Thermochemical and kinetic studies of a bisphenol antioxidant, *J. Org. Chem.* **2001**, *66*, 5456-5462.